The Electrical and Magnetic Properties of a Novel Two-Dimensional Antiferromagnet Based on BEDT–TTF: θ-$(BEDT–TTF)_2Cu_2(CN)[N(CN)_2]_2$

Tokutaro Komatsu, Hirohiko Sato,# Toshikazu Nakamura,## Nozomu Matsukawa, Hideki Yamochi, Gunzi Saito,* Masami Kusunoki,† Ken-ichi Sakaguchi,† and Seiichi Kagoshima††

Department of Chemistry, Faculty of Science, Kyoto University, Kitashirakawaoiwake-cho, Sakyo-ku, Kyoto 606-01

†Institute for Protein Research, Osaka University, Yamadaoka, Suita, Osaka 565

††Department of Pure and Applied Sciences, College of Arts & Sciences, The University of Tokyo, Komaba, Meguro-ku, Tokyo 153

(Received March 17, 1995)

A crystal-structure analysis and a band calculation, as well as conductivity, thermoelectric power, ESR, and static susceptibility measurements were performed on the new BEDT–TTF salt, θ-$(BEDT–TTF)_2Cu_2(CN)[N(CN)_2]_2$. This salt has a unique polymerized anion comprising infinite Cu–N-$(CN)_2$–Cu double helices bridged by disordered CN groups. Although the two-dimensional arrangement of crystallographically equivalent $BEDT–TTF^{+0.5}$ cations provides a two-dimensional closed Fermi surface within the tight-binding approximation, this salt is semiconductive even at room temperature, probably due to a strong electron correlation in this system. A semiconductor–semiconductor transition has been observed around 220 K. Below 220 K the electronic system is represented as a Mott insulator and a two-dimensional Heisenberg antiferromagnet. Rapid decreases in the ESR line width and spin susceptibility below 50 K indicate the existence of an additional magnetic transition.

BEDT–TTF (bis(ethylenedithio)tetrathiafulvalene) salts have afforded a wide variety of physical properties, including: superconductivity,[1] spin-density wave transitions,[2,3] magnetic oscillations,[4] Mott–Hubbard insulating states,[5—7] and the spin-Peierls transition.[8] Especially, BEDT–TTF has provided the largest number of molecular superconductors, namely, more than twenty salts. The resemblance of their physical and structural features with copper oxide superconductors has attracted keen interest. The similarities of these compounds are, for example, two-dimensional layered structures, the anisotropy of superconducting parameters (e.g. coherence length[9,10] and penetration depth,[9,11,12]) and the linear relation between the superconducting transition temperature (T_c) and the Fermi energy.[13]

Among BEDT–TTF based superconductors, more than ten salts have polymerized anions. The advantages of using polymerized anions to design a new BEDT–TTF based superconductor are: 1) a rigid anion structure that provides a low thermal contraction, resulting in a high density of states at low temperatures, and 2) a self-constructive anion that can take the initiative during crystal formation; by an adequate choice of the anion species the arrangement of BEDT–TTF molecules can be directly controlled.[14]

On the other hand, eight magnetic insulators have been reported up to now: four α' salts,[5—7] one β' salt,[15,16] two α salts[15,16] (these two salts are classified in α' according to the definition of H. Kobayashi), and the triclinic phase of BEDT–TTF·TCNQ.[17,18] In common, they show relatively strong dimerization; the calculated Fermi surface of the former two modifications is one-dimensional, while that of the latter two is two-dimensional.

In a search for BEDT–TTF superconductors with a polymerized anion of the X^-–M^+–X^- type, where X^- and M^+ represent a pseudohalogen and a tri-coordinative transition metal, respectively, we have synthesized two new superconductors, κ-$(BEDT–TTF)_2Cu(CN)[N-(CN)_2]$ (T_c=11.2 K) and κ'-$(BEDT–TTF)_2Cu_2(CN)_3$

#Present address: Department of Chemistry, Tokyo Institute of Technology, Ookayama, Meguro-ku, Tokyo 152.
##Present address: Department of Physics, Gakushuin University, Mejiro, Toshima-ku, Tokyo 171.

($T_c = 3.8$ K).[19] During the electrocrystallization of these salts the title compound was harvested simultaneously. In this paper, the synthesis as well as the structural, transport, and magnetic properties of this new BEDT–TTF salt are reported.

Experimental

Black flattened needles having a rhombus section of θ-(BEDT–TTF)$_2$Cu$_2$(CN)[N(CN)$_2$]$_2$ were prepared by electrocrystallization from a solution containing BEDT–TTF, Cu^+, CN^-, and $N(CN)_2^-$ under the galvanostatic condition and an N_2 atmosphere. As the solvent, (a) benzonitrile (BN), (b) 1,1,2-trichloroethane (TCE), (c) tetrahydrofuran (THF), (d) the mixed solvent of BN and TCE, and those containing ca. 10 vol% ethanol (EtOH) were used. In the following part, the solvent containing EtOH is denoted by an asterisk. The employed combination of electrolytes included: (1) CuCN+NaN(CN)$_2$+18-crown-6 (18-C-6), (2) CuN(CN)$_2$+KCN+18-C-6, (3) CuCN+tetraphenylphosphonium dicyanoamide ($Ph_4PN(CN)_2$). The supporting electrolytes were purified by previously described methods.[19] A small portion of water and/or excess ethanol seem(s) to favor the growth of the title compound. The crystal used for the X-ray structure analysis was grown in (b*)+(1), i.e., the TCE (16ml)+EtOH (2 ml) solution of BEDT–TTF (7 mg)+CuCN (22 mg)+NaN(CN)$_2$ (17 mg)+18-C-6 (41 mg). The conductivity at ambient pressure was measured on crystals harvested from the following five combinations of electrolytes and solvents: (b*)+(1), (c*)+(1), (a)+(2), (a*)+(3), and (d*)+(3). The other measurements were performed on crystals obtained from the electrolysis of BEDT–TTF in (a*)+(3): BEDT–TTF (35 mg), $Ph_4PN(CN)_2$ (210 mg) and CuCN (90 mg) in a mixture of BN (90 ml) and EtOH (10 ml). The lattice parameters of the crystals of this batch were the same as those of the crystal used for the structure analysis.

The X-ray crystal data at room temperature were collected with graphite monochromated Mo $K\alpha$ radiation on a Rigaku AFC-4 four-circle diffractometer. The observed 6003 reflections were averaged to 1569 unique, allowed ones, of which 1336 reflections ($2\theta < 50^\circ$, $F_o > 2\sigma(F_o)$) were used for the full-matrix least-squares refinement of a model (141 variables) obtained by direct methods.[20] The final R value was 5.56%. The diffuse X-ray photographs were taken by the monochromatic Laue method.[21]

An extended Hückel tight-binding band calculation was carried out with the usual procedure.[22] The transfer integral (t) between each pair of molecules is assumed to be proportional to the overlap integral (S), $t = ES$, where E is a constant of -10.0 eV. The HOMO band of BEDT–TTF was assumed to be 3/4 filled (BEDT–TTF$^{+0.5}$) based on the chemical formula of the salt with Cu^+.

The pressure dependence of the conductivity along the c-axis was measured by a four-probe method using a clamp-type pressure cell. Gold wires (Tanaka Densi Kogyo, 99.99%, 10 μmϕ) were glued to a crystal with gold paste (Tokuriki Chemical, No. 8560-1A) as electrodes. The pressures were determined by the change in the resistance of a manganin wire. The temperature was measured with a Pt resistance thermometer, which was also used for thermoelectric power measurements. The data below 150 K could not be measured because of the high resistance of the samples and the limitation of the constant-current source.

The thermoelectric power (TEP) of the single-crystal sample was measured by the following technique. To one end of the sample, an AuFe wire and a chromel wire (Ishikawa Sangyo, TAU7-003 (0.07%Fe) and TUKP-003, 0.076 ϕ) were attached with gold paste; also, a heat sink comprising an electrically insulated Cu block with a heater was glued using GE varnish. The other end of the sample was suspended and attached only with an AuFe wire and a chromel wire using gold paste. This apparatus releases the sample from the tension caused by the thermal anchors, and can give the exact temperature gradient of the sample. The TEP's of the sample measured with AuFe wires and chromel ones were recorded independently, and the temperature gradient was calculated from the difference between these two values, which is precisely the TEP of the AuFe–chromel thermocouple. The generated temperature gradient was less than 0.5 K. Subtracting the absolute TEP of chromel (calibrated by using Pb[23]) from the TEP of the sample measured with chromel wires, the absolute TEP of the sample was obtained.

The sample used for measuring the temperature and angular dependence of the ESR spectra was a single crystal having the dimensions of $2.2 \times 0.3 \times 0.1$ mm^3. The crystal axes of this sample were determined by its morphology, and were confirmed by the subsequent X-ray diffraction measurement. The room-temperature spin susceptibility was determined for compiled crystals of 0.95(2) mg. The sample was placed in a cylindrical cavity in the TE_{011} mode, where the microwave electric field and the static magnetic field were in the horizontal direction. The ESR spectra were recorded over the temperature range from 1.9 to 300 K with a JEOL JES-RE2X X-band ESR spectrometer equipped with an Oxford Instruments ESR-910 cryostat and an ITC4 temperature controller. The temperature was measured with an AuFe–chromel thermocouple calibrated by using a carbon-glass resistance thermometer. Since in this apparatus the temperature of the cavity was kept almost constant, regardless of that in the cryostat, the spin susceptibility of the reference sample (Mn^{2+}/MgO) was assumed to be independent of the sample temperature. Therefore, after the intensity variation of the sample due to the changes in the modulation width and amplitude was corrected, a further correction for changes in the resonance condition of the cavity was performed by using the intensity of the reference signal as a standard. In determining the absolute value of the spin susceptibility of the sample, $CuSO_4 \cdot 5H_2O$ (recrystallized from water, 1.94 mg) was used as a standard. As for the magnitude of the spin susceptibility of the standard sample at 300 K, a value of 6.30×10^{-6} emu g^{-1} was employed.[24] The microwave frequency and the magnetic field were measured by an Advantest R5372 frequency counter and an ECHO Electronics EFM-200AX field meter, respectively. The measured magnetic field and microwave frequency gave the same g-factor for Li^+TCNQ^- as the reported one (2.0026). The obtained first derivative ESR signal (2048 data points) was fitted to an appropriate mixture of Lorentzian absorption and dispersion by a least-squares method (6 parameters[25]). Since it was difficult to estimate the extent of the skin effect due to the limited size of the crystal, the spin susceptibility was evaluated only for the cases in which the observed line shape was not distorted.

A Quantum Design MPMS2 SQUID magnetometer was used to collect magnetization data between 5 K and 300 K at a fixed field of 500 G (1 G=0.1 mT). Randomly oriented small crystals of the title compound (16.38 mg) were wrapped in polyethylene film and held in a plastic drinking straw. The core susceptibility (χ_{core}) was estimated by Pascal's law, $\chi_{core}=-5.05\times10^{-4}$ emu mol^{-1}.[26]

Results and Discussion

Crystal Structure: The crystal of θ-(BEDT–TTF)$_2$Cu$_2$(CN)[N(CN)$_2$]$_2$ belongs to the orthorhombic non-centrosymmetric space group I222 with $a=11.088(2)$, $b=38.837(5)$, $c=4.2010(5)$ Å, $V=1809.1(4)$ Å^3, and $Z=2$. The atomic parameters are listed in Table 1. The observed density and compositions are 1.94 (1.934), C=28.42—28.57% (28.49), H=1.41—1.59% (1.52), N=9.35% (9.31), respectively. The calculated values for $C_{25}H_{16}N_7S_{16}Cu_2$ are indicated in the parentheses. The crystal structure viewed along the c-axis is shown in Fig. 1. The a- and b-axes coincide with the short- and long-diagonal of the section of the needle, respectively. The c-axis is parallel to the needle axis. This salt contains two kinds of layers. The layers of BEDT–TTF donor molecules and that of polymeric Cu$_2$(CN)[N(CN)$_2$]$_2^-$ anion units pile up alternatingly along the b-axis. The fact that the crystal grows more rapidly in the direction perpendicular to the conducting ac plane ($//b$ axis) than in one parallel direction ($//a$ axis) is in contrast to the ordinary conducting salts, in which the most developed plane is usually parallel to the conducting plane.

In the donor layer, BEDT–TTF molecules form a uniform stack along the c-axis with an interplanar distance of 3.8 Å and a θ-type arrangement (Fig. 2), in which

Table 1. Final Atomic Coordinates and Equivalent Isotropic Thermal Parameters of the Non-hydrogen Atoms

Atom	x	y	z	B_{eq}[a)]/Å^2
S1	0.1464 (2)	0.34407 (6)	0.3310 (9)	2.70
S2	0.1208 (2)	0.26898 (6)	0.3579 (9)	3.04
S3	0.1189 (2)	0.18586 (6)	0.3469 (9)	2.73
S4	0.1462 (2)	0.11040 (6)	0.3370 (9)	2.82
C5	0.0690 (8)	0.3791 (2)	0.534 (3)	2.44
C6	0.0548 (9)	0.3091 (2)	0.4380 (3)	2.27
C7	0.00000 (0)	0.2096 (3)	0.50000 (0)	2.35
C8	0.00000 (0)	0.2450 (3)	0.50000 (0)	2.24
C9	0.0553 (8)	0.1455 (2)	0.435 (2)	1.86
C10	0.0669 (8)	0.0750 (2)	0.532 (3)	2.45
Cu	0.2212 (2)	0.00000 (0)	0.00000 (0)	3.96
C21	0.051 (1)	0.00000 (0)	0.00000 (0)	3.04
N21	0.051 (1)	0.00000 (0)	0.00000 (0)	3.96
N22	0.50000 (0)	0.0577 (3)	0.50000 (0)	4.29
C23	0.415 (1)	0.0420 (3)	0.358 (3)	3.46
N24	0.3318 (9)	0.0320 (3)	0.222 (3)	4.83

a) B_{eq} is defined by the following equation, $B_{eq}=\frac{3}{4}(\sum_i\sum_j B_{ij}\boldsymbol{a}_i\cdot\boldsymbol{a}_j)$.

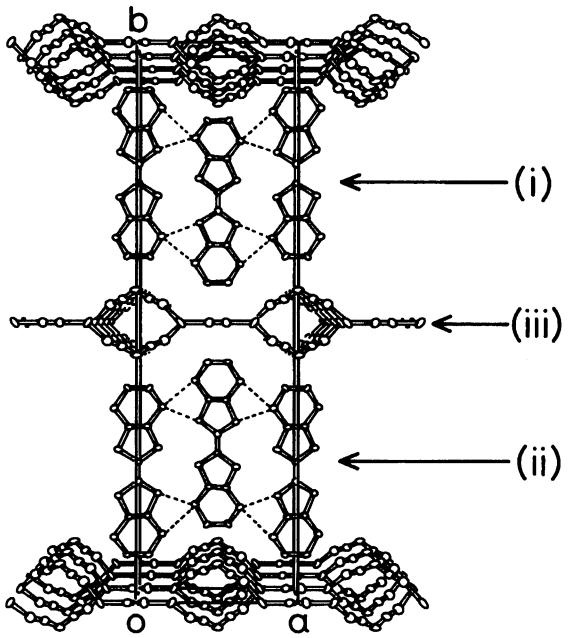

Fig. 1. The crystal structure of θ-(BEDT–TTF)$_2$Cu$_2$(CN)[N(CN)$_2$]$_2$ viewed along the c-axis. The intermolecular S···S contacts shorter than the sum of the van der Waals radii (3.6 Å) are indicated by broken lines. The upper- and the lower BEDT–TTF layers and the central anion layer are denoted as layer (i), (ii), and (iii), respectively.

every two donor molecules repeat along the long molecular axis, just as observed in θ-(BEDT–TTF)$_2$I$_3$.[27] For conciseness, hereafter 2:1 BEDT–TTF salts are written without (BEDT–TTF)$_2$, e.g., θ-(BEDT–TTF)$_2$I$_3$ is abbreviated as θ-I$_3$. The molecular planes are parallel to each other within the stack, and make an angle of 48° between the stacks (Fig. 2b). One BEDT–TTF molecule is surrounded by six molecules, among which four molecules in the neighboring stacks are generated by a two-fold screw operation, whereas the other two in the same stack are related by the c-axis translation. The angle between the molecular short axis and the stacking direction is 66° (Fig. 2b), while that of metallic θ-I$_3$ salt is 40°.[27] In the TTF-based molecular conductors, this angle is known to play the most crucial role in determining the transfer integral between the neighbouring molecules in a stack,[22] and, consequently, the electronic structure. Therefore, the qualitative difference of the transport properties between these salts is expected to have some relation to this quantitative variation of the donor arrangement. We will discuss this subject in more detail in the following section. As shown in Fig. 1, four S···S contacts shorter than the sum of the van der Waals radii (3.6 Å) are present for a donor pair between the stacks to form a conducting two-dimensional network in the ac plane, while no such atomic contacts are found within the stack. The intermolecular S···S contacts shorter than 3.6 Å are listed in Table 2. There exists merely one kind of interstack donor configura-

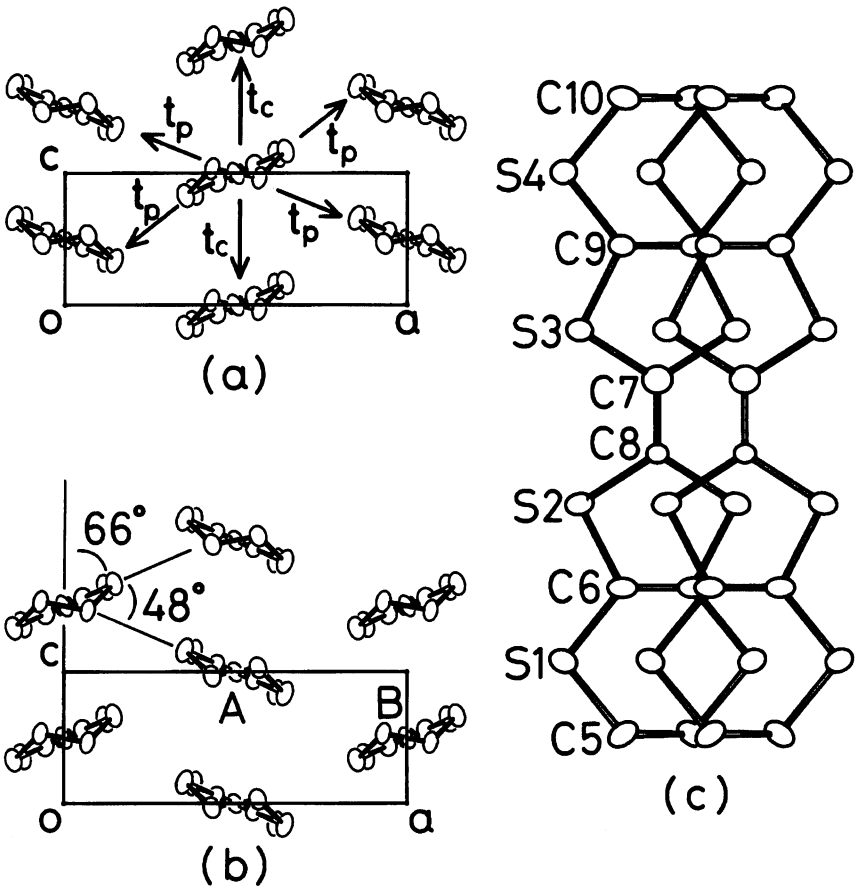

Fig. 2. The *b*-axis projection of the two BEDT–TTF layers of θ-(BEDT–TTF)$_2$Cu$_2$(CN)[N(CN)$_2$]$_2$: (a) The upper layer (i) and (b) the lower layer (ii) shown in Fig. 1. The intermolecular S···S contacts between molecules A and B shorter than 3.6 Å are summarized in Table 2. t_c and t_p represent the intra- and interstack transfer integral, respectively. (c) The intrastack BEDT–TTF configuration viewed perpendicular to the molecular plane and the numbering scheme of the atoms of the BEDT–TTF molecule.

Table 2. Intermolecular S···S Distances (Å) Shorter Than the Sum of the van der Waals Radii (3.6 Å) from the Molecule A to the Molecule B (Fig. 2)

S1–S4	3.567 (4)	S1–S3	3.502 (4)
S3–S1	3.581 (4)	S4–S1	3.596 (4)

tion, which gives the interstack transfer integral (t_p), as indicated in Fig. 2a. The donor molecules in a stack slide solely in the direction of their short molecular axes (Fig. 2c), just like such BEDT–TTF salts as α-I_3,[28] α″-Cu_5I_6,[29] α″-$CsHg(SCN)_4$.[30] Only the half part of the donor molecule is crystallographically unique; the other half is generated by a two-fold rotation operation around the central C=C bond. The molecular long axis is parallel to the *b*-axis, and the molecular short axis rotates 24° with respect to the *a*-axis. The bond lengths and angles are summarized in Table 3. The central C_6S_8 skeleton of a BEDT–TTF molecule in the crystal is fairly planar, where the atoms are located within 0.05 Å from the least-squares plane derived from the C_6S_8 group. The BEDT–TTF molecule has an eclipsed conformation of the terminal ethylene groups with no

Table 3. Bond Lengths (Å) and Angles (°)

C5–C5	1.56 (2)	C5–S1	1.82 (1)
S1–C6	1.75 (1)	C6–C6	1.32 (2)
C6–S2	1.76 (1)	S2–C8	1.74 (3)
C7–C8	1.37 (5)	C7–S3	1.73 (3)
S3–C9	1.757 (9)	C9–C9	1.34 (2)
C9–S4	1.745 (9)	S4–C10	1.83 (1)
C10–C10	1.51 (2)	C21–N21	1.141 (8)
C21–Cu	1.882 (4)	Cu–N24	1.98 (1)
N24–C23	1.15 (2)	C23–N22	1.27 (1)
C5–C5–S1	112.1 (7)	C5–S1–C6	100.7 (5)
S1–C6–C6	129.3 (8)	S1–C6–S2	113.4 (5)
C6–C6–S2	117.3 (7)	C6–S2–C8	95 (1)
S2–C8–S2	115 (2)	S2–C8–C7	122 (3)
C8–C7–S3	122 (3)	S3–C7–S3	116 (2)
C7–S3–C9	95 (1)	S3–C9–C9	116.9 (7)
S3–C9–S4	114.6 (5)	C9–C9–S4	128.6 (7)
C9–S4–C10	101.8 (5)	S4–C10–C10	113.2 (7)
C21–Cu–N24	128.3 (4)	N24–Cu–N24	103.5 (5)
Cu–N24–C23	160 (1)	N24–C23–N22	171 (1)
C23–N22–C23	122.7 (8)		

disorders.

The anion layer is constructed of double helices of –Cu–NCNCN– inifinite chains bridged by CN groups (Fig. 3). With the present crystal system, these CN groups are crystallographically disordered. The positions of N21 and C21 were assumed to be the same; only their thermal parameters were refined separately. We could not determine whether these CN groups are ordered or not for the following reason. The atomic scattering factors of the CN group are much smaller than that of the rest of atoms. Our experimental accuracy is not sufficient to detect such a small difference of the structure factor.

The Cu atom is coordinated by two terminal nitrogen atoms of dicyanoamides (N24) and a disordered CN group (C/N21) in a triangular-planar form. This type of coordination is often observed for Cu^{1+} complexes. The bond angles around the Cu atom deviate from 120° (Table 3). This fact indicates that this two-dimensional polymeric anion involves structural frustration.

Another feature of this anion structure is that there are two systems of the polymeric anion separated from each other within one anion layer. No atomic contacts shorter than the sum of the van der Waals radii were found between them. They are indicated with open and closed bonds in Fig. 3. The thickness of the anion layer is 7.6 Å at the double-helix part and 3.4 Å at the bridging CN group. This is a rather large value compared with other BEDT–TTF salts, e.g., less than 3.7 Å for such superconductors with T_c above 10 K as κ-$Cu(NCS)_2$ and κ-$Cu(CN)[N(CN)_2]$ (the sum of the van der Waals radii of anion atoms), ca. 4 Å for triiodide salts, and 6.8 Å for α-$KHg(SCN)_4$ salt[31]). The inside diameter of the double helices is about 0.8 Å, which is comparable to the ionic radii of metal cations.

One BEDT–TTF molecule has five hydrogen-anion contacts comparable to the sum of the van der Waals radii (H–N=1.75 Å, H–C=1.9 Å). As one can see in Fig. 4, the equatorial terminal ethylene hydrogens of the BEDT–TTF molecules are allocated in the zigzag channel formed between the anion polymers (anion channel). It should be noted that due to the helical part of the anion chain, the direction of the anion channel is different for the upper part and the lower part of the anion layer, that is, approximately $(1,0,\bar{1})$ for the former (Fig. 4a) and (1,0,1) for the latter (Fig. 4b). This feature of the anion layer corresponds to the direction of the short molecular axes of the BEDT–TTF molecules, which alternate along the b-axis. In other words, this rigid polymeric anion structure seems to favor the θ-type donor arrangement. The direction of the donor stack (i.e., (0,0,1)) does not agree with that of the anion channel. This situation is somewhat different from that in θ-I_3, where the two directions are parallel to each other.[14]

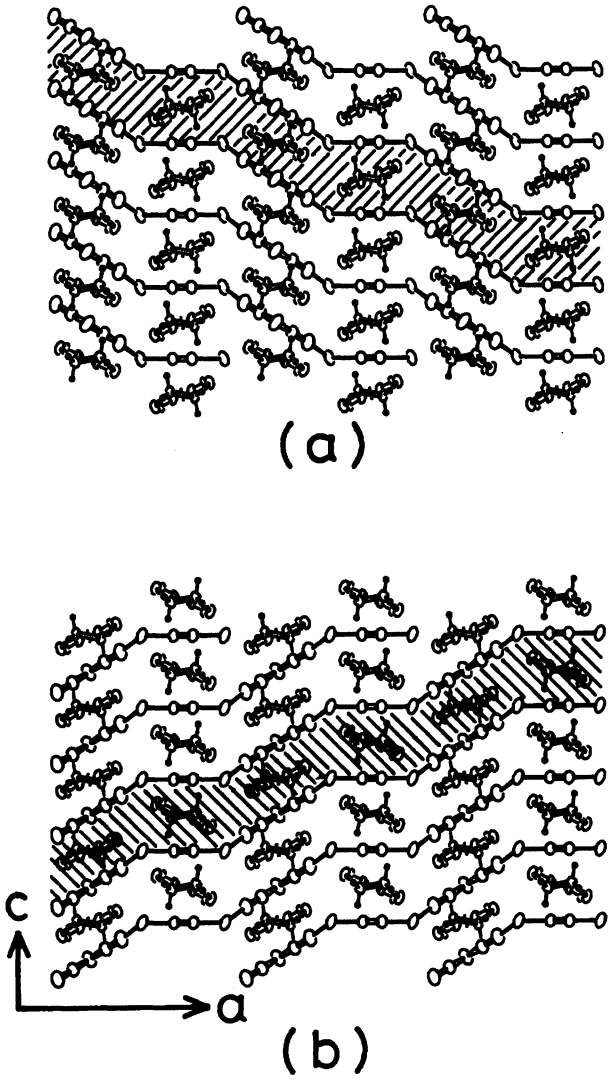

Fig. 4. (a) The b-axis projection of the upper BEDT–TTF layer (i) of θ-$(BEDT–TTF)_2Cu_2(CN)[N(CN)_2]_2$ shown in Fig. 1 with the upper part of the anion layer (iii). For clarity, the lower part of dicyanoamides are omitted. (b) The lower BEDT–TTF layer (ii) viewed through the anion layer (iii) without the upper part of dicyanoamides. The shaded region indicates the channel in the anion layer, whose direction is different between the upper and the lower part of the anion layer.

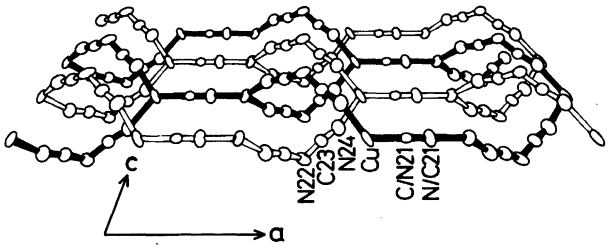

Fig. 3. The perspective view of the anion layer of θ-$(BEDT–TTF)_2Cu_2(CN)[N(CN)_2]_2$. The two separate polymeric anion systems are shown by open and closed bonds.

Band Calculation: Figure 5 shows the energy dis-

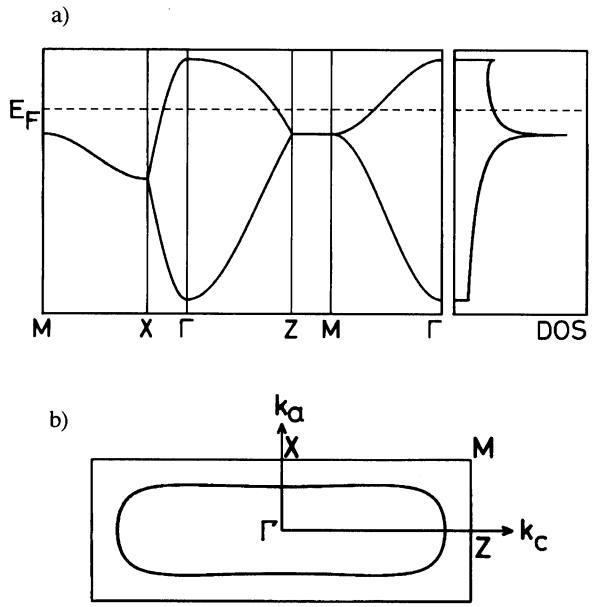

Fig. 5. The calculated energy dispersion and density of states (a) and the Fermi surface (b) of θ-(BEDT–TTF)$_2$Cu$_2$(CN)[N(CN)$_2$]$_2$.

persion, the energy dependence of the density of states (DOS) and the Fermi surface (FS) of the title compound. The energy dispersion is represented by the formula

$$E(k_a, k_c) = 2t_c\cos(k_c \cdot c) \pm 4t_p\cos(k_a \cdot a/2)\cos(k_c \cdot c/2), \quad (1)$$

with the intra- and interstack transfer integrals $t_c = -30.0$ meV and $t_p = 79.4$ meV (see Fig. 2), respectively. For a comparison, the energy dispersion and the DOS of θ-I_3 salt based on the averaged orthorhombic structure are redrawn after H. Kobayashi et al. (Fig. 6).[27] The energy dispersion of θ-I_3 salt is also expressed by Eq. 1 with $t_c = 64$ meV and $t_p = 42$ meV. In both cases, the k_a-dependence of the eigenenergy disappears at the Z–M line at the zone boundary, and the energy dispersion becomes quasi-one-dimensional. This is because the second term of Eq. 1 vanishes. This singular point of the θ-type band dispersion corresponds to the maximum position of DOS.

The energy dependence of the DOS of the title compound is inversed with respect to that of θ-I_3 salt due to the opposite sign of t_c. As a consequence, the Fermi level of the title compound is situated in the vicinity of the maximum position of DOS. The calculated DOS at the Fermi level, band width, and the energy difference between the Fermi level and the singular point are 2.21 states/eV·molecule·spin, 0.65 eV and 68 meV for the title compound and 1.52 states/eV·molecule·spin, 0.46 eV and 248 meV for θ-I_3 salt, respectively. As mentioned in the preceding section, these differences between these salts derive from the different donor configuration within the stack.

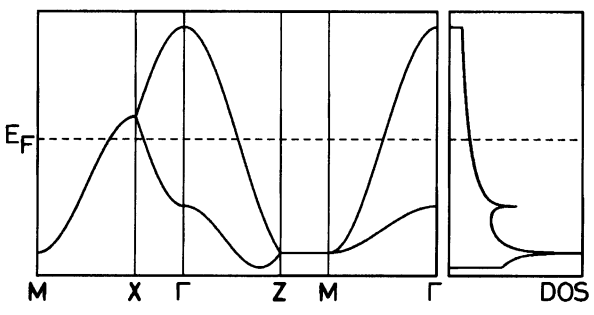

Fig. 6. The energy dispersion and density of states of θ-(BEDT–TTF)$_2$I$_3$ redrawn after H. Kobayashi et al.[27]

The other important point of the above-mentioned calculation is that the title compound is more anisotropic in the conducting plane than θ-I_3 salt; that is, the title compound possesses a racetrack-shaped FS with the flat side parallel to the k_c direction, while that of θ-I_3 salt is a nearly isotropic oval one. This flat part of FS can induce a lattice distortion along the *a*-axis and a partial nesting of the FS.

In summary, a band calculation based on the room-temperature crystal structure asserts that the title compound should be metallic. In addition, the pseudo-one-dimensional singular point lying just below the Fermi level indicates that a subtle change of the crystal structure can easily change the electronic system into a quasi-one-dimensional one, and eventually into an insulating state.

Conductivity: An Arrhenius plot of the conductivities along the *c*-axis (σ_c) under the pressures of ambient pressure (AP) and 0.9 GPa are shown in Fig. 7a. The temperature dependence of the conductivity remains semiconductive up to 300 K at 0.9 GPa and 400 K at AP. The energy gaps (E_g) at room temperature are 0.17—0.19 eV at AP and 0.12 eV at 0.9 GPa. The magnitude of E_g at AP is the same for all the crystals obtained from the above-mentioned five different routes. The conductivity at room temperature (σ_{RT}) ranges from 1.7 to 16 S cm^{-1}, which varies little with the pressure. At ambient pressure, σ_{RT} parallel to the *a*-axis is of the same order as that parallel to the *c*-axis.

The apparent energy gap is not constant, but gradually grows when the temperature is lowered. It is thus tempting to assume that the metallic nature of the two-dimensional BEDT–TTF layers is hampered by the random potentials of some disorder. However, the temperature dependence of conductivity above 220 K can not be represented by the formula of a variable range hopping model, $\sigma(T) = \sigma_0 \exp[-(T_0/T)^\alpha]$, where $\alpha = (d+1)^{-1}$ and d is the dimensionality of the system. The observed behavior is rather well fitted with an unrealistic value of $\alpha \approx 3$. Therefore, the semiconductive behavior is not caused by any disorder. The temperature dependence of the energy gap may be brought about by a fluctuation of the transition at 220 K.

The following two facts indicate that this semiconductive behavior is not due to a surface decomposi-

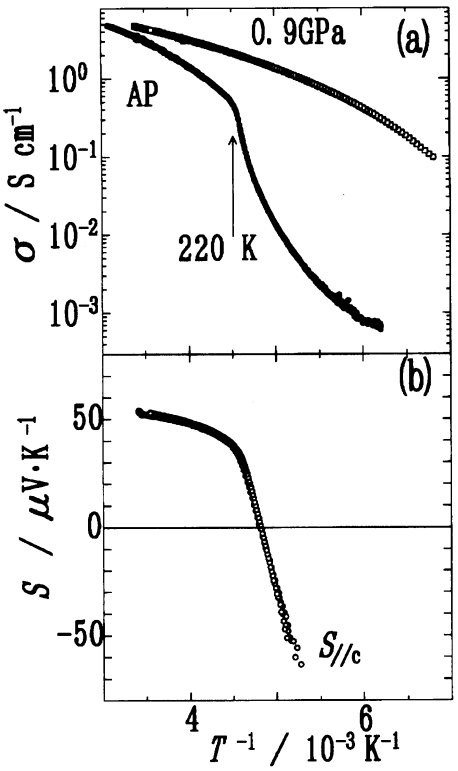

Fig. 7. (a) The conductivity of θ-(BEDT–TTF)$_2$Cu$_2$(CN)[N(CN)$_2$]$_2$ measured under ambient pressure (AP, filled circles) and 0.9 GPa (open squares). The arrow indicates the transition at 220 K. (b) The thermoelectric power of θ-(BEDT–TTF)$_2$Cu$_2$(CN)-[N(CN)$_2$]$_2$ measured along the c-axis.

tion: i) the samples showed a semiconducting behavior, even when the electrodes were made with silver paste or made on gold pads evaporated on a sample (it is unlikely that the reaction between the sample and the electrodes prevents the sample from showing metallic properties), and ii) the asymmetric ratio of the ESR line shape, which reflects the electrical conductivity, decreased with decreasing conductivity and converged to unity at temperatures below 220 K (vide infra).

There is a semiconductor–semiconductor transition at 220 K under ambient pressure, which is not observed under 0.9 GPa. The transition temperature is defined as the temperature at which the slope of the Arrhenius plot of σ_c suddenly changes. At the transition temperature the apparent energy gap increases (0.6—0.7 eV); however, since there is no linear part in the plot, the accurate magnitude of the gap is not determined. α-IBr$_2$ salt, whose magnetic properties resemble those of the title compound, also exhibits a similar semiconductor–semiconductor transition around 200 K.[16]

Thermoelectric Power: Around room temperature, a positive TEP was observed (Fig. 7b) along the c-axis. The positive TEP in the conducting plane indicates that the conduction in the donor sheet is dominated by hole carriers; this idea is consistent with a hole pocket in the k_a–k_c plane expected from the formal oxidation +0.5 of the BEDT–TTF. The transition at 220 K is clearly observed as a rapid decrease of TEP. Below 220 K, TEP varies as T^{-1}, which is a typical semiconducting behavior. The obtained energy gap (ca. 0.3 eV) is temperature independent and comparable to that derived from the conductivity data. Above 220 K, TEP does not show a T^{-1} temperature dependence. Therefore, the title compound is not an ordinary semiconductor above 220 K.

The TEP saturates toward 52 $\mu V K^{-1}$ along the c-axis at around room temperature. This value is slightly larger than that of metallic BEDT–TTF salts, and indicative of the existence of a strong electron correlation, because it is known that for a system with a carrier density (ρ) of 0.5 holes/site, TEP saturates towards 60 $\mu V K^{-1}$ when the on-site Coulomb repulsion (U) is larger than both $k_B T$ and the band width.[32]

ESR and Static Susceptibility: The observed ESR signal is a single Lorentzian curve as long as the microwave electric field (E) is perpendicular to the ac plane; otherwise, the signal contains a dispersion component above about 200 K. At room temperature, the distortion ratio (A/B) between the maximum and minimum of the derivative of absorption is 1.1, which decreases with decreasing temperature, and becomes unity below ca. 200 K (Fig. 8). The magnitude of d.c. conductivity is rather small to account for the observed distortion of the ESR line shape; that is, taking $\sigma_a \approx \sigma_c \approx 10$ S cm^{-1}, the resultant skin depth is about 0.3 mm, which is comparable to the crystal size (the area of the conducting plane was 0.1×2.2 mm^2).

The angular dependencies of the g factor and the peak-to-peak line width (ΔH) observed at room tem-

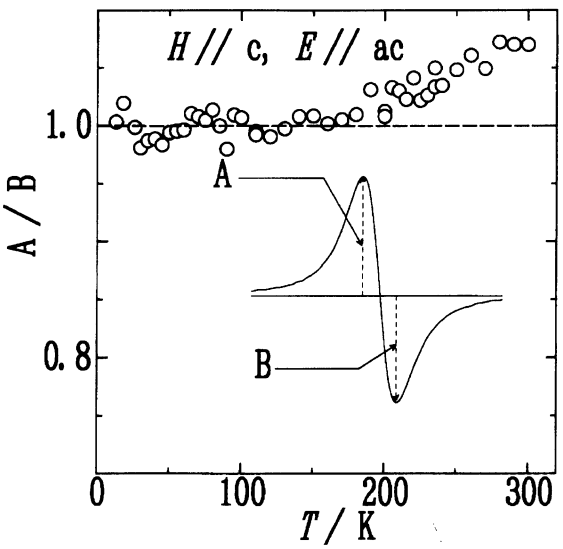

Fig. 8. The temperature dependencies of the ratio A/B between the maximum and minimum of the derivative of ESR absorption line with the static field H parallel to the c-axis and the microwave electric field E parallel to the ac (conducting) plane.

perature are shown in Fig. 9. The circles and squares represent the data measured by rotations of the static magnetic field (H) from the c-axis to the a-axis and from the b-axis to the a-axis, respectively. In both cases, maximum and minimum g factors are observed when H is applied parallel to the crystal axis, namely, $g_{//a}$= 2.005, $g_{//b}$=2.013, and $g_{//c}$=2.002. The principal values of the g tensor of BEDT–TTF salts are known to be g_1= 2.011—2.012, g_2=2.006—0.007, and g_3=2.002—2.003 for the directions of molecular long, short axis, and normal to the molecular plane, respectively. Their average ($\bar{g}$) is 2.006—2.007,[33] which is almost equal to that observed for the title compound ($\bar{g}$=2.0063). These observations suggest that the g factor of this salt is determined by the g tensor of the BEDT–TTF cation radical. The spin observed by the ESR measurements is thus on the BEDT–TTF molecule. The angular dependence of ΔH is the same as that of the g factor; their values are $\Delta H_{//a}$=36, $\Delta H_{//b}$=56, and $\Delta H_{//c}$=34 G. These directions are nearly parallel to the molecular short axis, the long axis, and the direction normal to the molecular plane of BEDT–TTF, respectively.

Since no signal of localized Cu^{2+} (g=2.05—2.50) was observed down to 1.9 K, the copper atoms in the crystal are thought to be diamagnetic Cu^{+}. Therefore, the formal oxidation state of the BEDT–TTF is +0.5, which confirms the assumption of the 3/4 filled band.

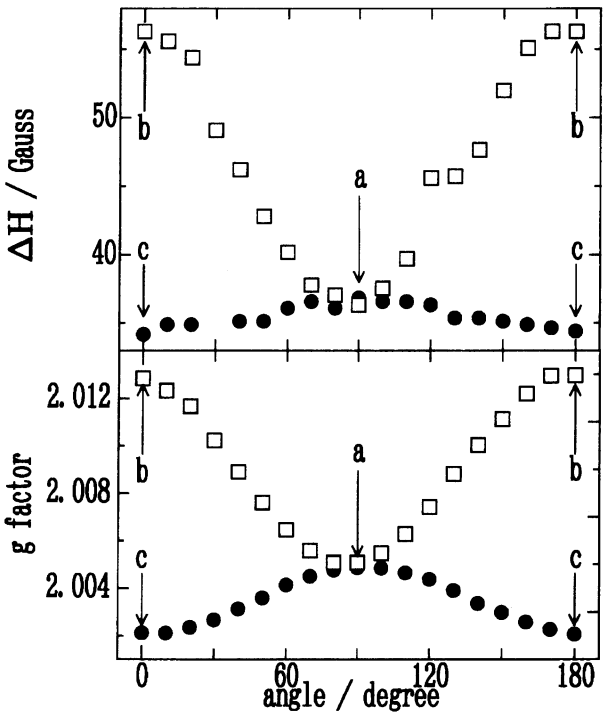

Fig. 9. The angular dependencies of the peak-to-peak line width ΔH and the g factor of θ-(BEDT–TTF)$_2$Cu$_2$(CN)[N(CN)$_2$]$_2$ at room temperature. Open squares and closed circles represent the data obtained by b–a–b and c–a–c rotation of the static field, respectively. 1 G equals to 0.1 mT.

The temperature dependencies of the g factor, the ΔH, and the spin susceptibility (χ_{spin}) measured with H approximately parallel to the b-axis and E to the ab plane, and with H parallel to the c-axis and E to the ac plane (the conducting plane) are shown in Fig. 10. A Lorentzian signal is observed from room temperature down to about 10 K, where another signal with almost the same g factor and a narrower line width starts to increase with decreasing temperature. Judging from its g factor, the origin of this additional signal seems to be some imperfection of the BEDT–TTF arrangement.

The g factor is almost temperature independent. The line width decreases slightly with decreasing temperature above about 250 K; it then drops rapidly down to ca. 230 K. This rapid change can be related to the transition observed by the conductivity and the TEP measurements. Considering the transport properties, one of the simplest interpretations is that the sudden decrease of ΔH corresponds to an extinction of the itinerant charge carriers, which eliminates the relaxation mechanism through charge-carrier scattering. Below the transition temperature ΔH is almost constant down to ca. 55 K, where it starts to decrease at a faster rate.

The χ_{spin} measured with H parallel to b is $9.3(2)\times10^{-4}$ emu mol^{-1} at room temperature, which is comparable to the BEDT–TTF based Mott insu-

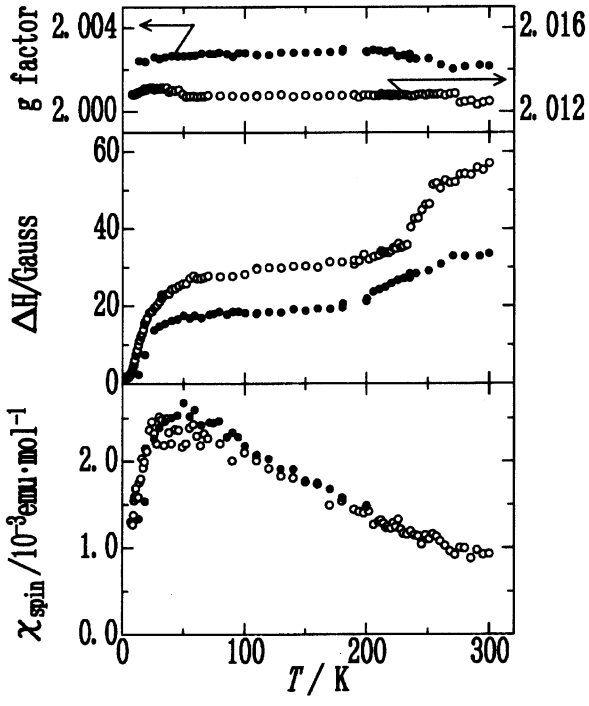

Fig. 10. The temperature dependencies of the g factor, peak-to-peak line width ΔH, and ESR spin susceptibility χ_{spin} of θ-(BEDT–TTF)$_2$Cu$_2$(CN)[N(CN)$_2$]$_2$ measured with the static field H parallel to the c (closed circles) and b-axes (open circles). 1 G equals to 0.1 mT. The χ_{spin} above 200 K measured with H parallel to the c-axis is not calculated because of the distortion of the observed signal.

lators with BEDT–TTF$^{+0.5}$, e.g. α'-$AuBr_2$ (9.0×10^{-4} emu mol^{-1}), α'-$CuCl_2$ (9.0×10^{-4} emu mol^{-1}), and α'-$Ag(CN)_2$ (9.3×10^{-4} emu mol^{-1}) salts,[6] and about two-times larger than metallic BEDT–TTF salts, for example, κ-$Cu(NCS)_2$ (4.6×10^{-4} emu mol^{-1}),[34] and β-I_3 (4.6×10^{-4} emu mol^{-1}),[35] etc. Below 200 K, χ_{spin} measured with H parallel to b and H parallel to c coincide with each other. In both directions, χ_{spin} increases monotonically from room temperature down to about 40 K, and then decreases. It should be emphasized that no prominent change in χ_{spin} has been observed at the transition temperature around 220 K, which has been confirmed by static susceptibility measurements (Fig. 11). In other words, the number of spins does not decrease at the transition temperature. Although this result apparently conflicts with the above interpretation of the ΔH decrement, if we attribute the source of the extinction of the itinerant charge carriers to the electron–electron repulsion, which is not favorable to a singlet state, but is able to localize carriers, we can settle the inconsistency between the carrier extinction and the constant number of spins. Therefore, this salt is regarded as being a Mott insulator in a wide sense, at least below 220 K.

By a static susceptibility measurement, the resulting χ_{spin} at room temperature is 9.8×10^{-4} emu mol^{-1}. This value is in fair agreement with that obtained by the ESR measurement within the experimental error. This fact again confirms that the oxidation state of the Cu is +1. No Curie tail of an impurity was observed.

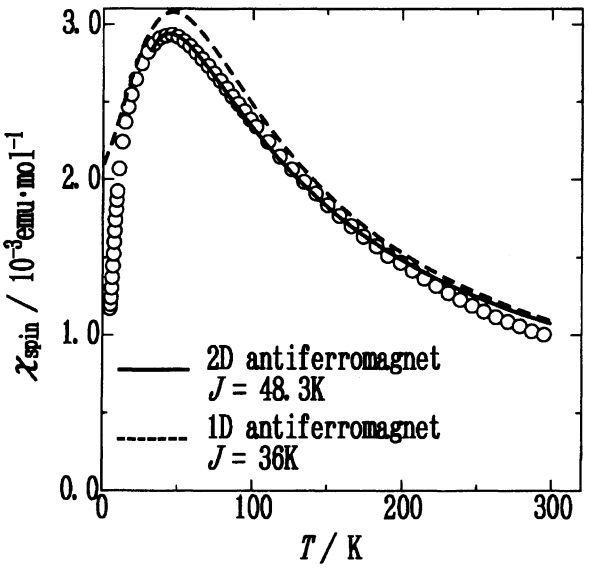

Fig. 11. The temperature dependence of the static susceptibility of the randomly oriented crystals of θ-$(BEDT–TTF)_2Cu_2(CN)[N(CN)_2]_2$. The core diamagnetism is subtracted. The solid and broken lines denote the calculated susceptibility for two-dimensional Heisenberg antiferromagnet with the exchange energy $J=48.3$ K and Bonner–Fischer model with $J=36$ K, respectively.

The broken line in Fig. 11 is the calculated susceptibility for a one-dimensional Heisenberg antiferromagnet (Bonner–Fischer model[36]), with the exchange energy between the adjacent sites $J=36$ K; the solid line is that for the two-dimensional quadratic-layer Heisenberg antiferromagnet[37] with $J=48.3$ K. The exchange energies of both cases are chosen so that the temperature of the susceptibility maximum coincides with the experimental value. In both cases, the experimental g factor of $\bar{g}=2.0063$ is used, and both $S=1/2$ and 0.5 spins/BEDT–TTF are assumed. The two-dimensional plot is a series expansion to six terms in J/T using the constants in the reference. Due to the limited number of terms used, the expansion in the two-dimensional model fails at temperatures below $T=0.9JS(S+1)$, and, therefore, the calculated values are plotted only above 32.6 K. Between 32.6 and 220 K the two-dimensional model completely agrees with the experimental values. Above 220 K the experimental values are slightly lower than that estimated by the two-dimensional model. This fact may be related to the high delocalization of charge carriers in this temperature region. Since the absolute magnitude of the susceptibility is determined by the fixed number of spins, the fact that the calculations are in good agreement with the experimental values suggests that all charges on the BEDT–TTF molecules are at a localized state with $S=1/2$ at least between 220 and 50 K.

Below 50 K, the rapid decrease of χ_{spin} with decreasing temperature is similar to that observed below a spin-Peierls transition. Although the strong $0.5c^*$ superstructure observed below 15 K (see below) also seems to support this idea, there are some difficulties. First, the χ_{spin} does not vanish, even at the lowest temperature measured. Second, since the oxidation state of BEDT–TTF is +0.5, the dimerization of BEDT–TTF cannot cause a singlet state by itself. A tetramerization of BEDT–TTF is necessary for a singlet state. Although one possible structural modulation is $0.25c^*$ superstructure, no diffuse streak corresponding to this periodicity was observed. Another possibility is that $0.5c^*$ modulation accompanies an interstack dimerization. Since there are two stacks of BEDT–TTF in a unit cell, this modulation causes only a symmetry lowering, and no superstructure would be observed.

Diffuse X-Ray Scattering: Owing to its high sensitivity, the monochromated Laue photograph exhibits very weak diffuse streaks due to the superstructure with a wave vector of $0.5c^*$ at room temperature; however, with the four-circle diffractometer no signals corresponding to the diffuse streaks were observed, even at 141 K. No other superstructure was found. The diffuse streaks condensed into spots as the temperature was lowered, and became intensely observable below 15 K in the monochromated Laue photograph (Fig. 12c), which indicates that there exists strong unit-cell size doubling. As has been mentioned, this lattice distortion

seems to cause a rapid decrease of the ESR line width and spin susceptibility below 50 K. On the other hand, there is no significant difference in the monochromatic Laue photograph between 240 and 200 K (Figs. 12a and 12b), in spite of the transition at 220 K observed by transport measurements. Therefore, this superstructure is not concerned with the transition at 220 K. As mentioned above, the origin of this lattice distortion does not seem to be electronic. Probably some structural instabilities, e.g., a reconstruction of polymeric anion networks, are the driving forces of this lattice distortion.

Summary

Based on the physical properties of the title compound we can define three temperature regions: a) $T>220$ K, b) 50 K$<T<220$ K, and c) $T<50$ K.

The specific features of region a) is rather high conductivity, broad ESR line width, and a very weak $0.5c^*$ distortion. The TEP does not show a T^{-1} temperature dependence, but a saturated behavior to 60 μV K^{-1} at around room temperature. These facts indicate that the carriers are fairly delocalized and, probably, in a weakly degenerated state.

In region b), the low-conductivity, T^{-1} dependence of TEP, a nearly constant ESR line width, and a very weak $0.5c^*$ distortion were observed. The temperature dependence of the χ_{spin} in region a) can be smoothly extrapolated into region b). This result indicates that the number of spins is not much affected by the transition at 220 K, at which the conductivity and TEP exhibit a distinct boundary between regions a) and b). These physical properties, together with the static magnetic susceptibility analysis, support that the carriers are strongly localized. They are also indicative of a Mott insulator with a half-filled band, which has been realized by dimerization in the case of the 2 : 1 BEDT–TTF salts mentioned in the introduction. However, since the $0.5c^*$ distortion is not distinct in the title compound, a precise structure analysis is necessary in this temperature region to assert the dimerization of BEDT–TTF molecules.

The transport properties in region c) has not yet been clarified because of the very low conductivity. Region c) is distinguished from region b) by a strong $0.5c^*$ distortion, and a rapid decrease of both the ESR line width and the spin susceptibility. The origin of the lattice distortion does not seem to be a spin-lattice interaction.

The possible origins of the semiconductive behavior of this compound, which has a two-dimensional uniform segregated stacking of +0.5 charged BEDT–TTF molecules, are considered to be as follows. One possibility is that electron localization is caused by a strong disorder. Currently, although the orientation of the CN groups in the anion layer has not been determined, there are some difficulties to explain the activated conductivity at room temperature only based on the disorder

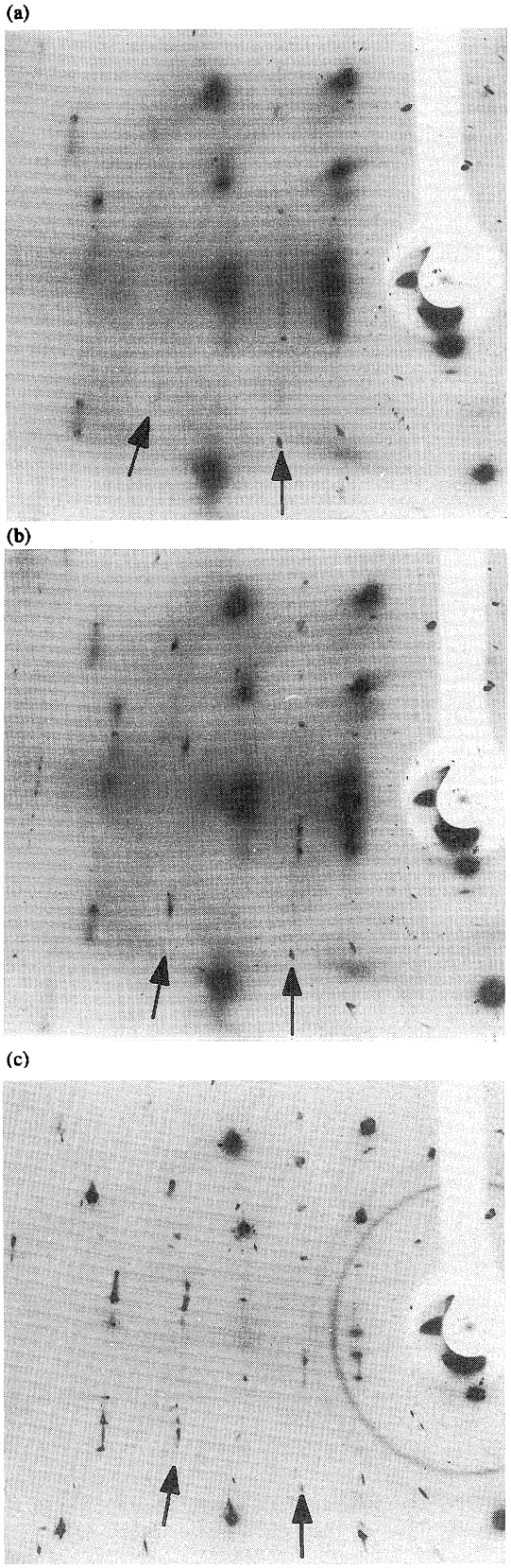

Fig. 12. The monochromatic Laue photographs of θ-(BEDT–TTF)$_2$Cu$_2$(CN)[N(CN)$_2$]$_2$ taken at (a) 240 K, and (b) 200 K, and (c) below 15 K. The *c*-axis is in the horizontal direction. The arrows indicate the diffuse spots or streaks.

of the CN groups. First, the temperature dependence of the conductivity does not follow the variable-range hopping model, which is expected for a disordered conductor. Second, if some kind of disorder were the origin of the semiconducting behavior, such conductivity parameters as σ_{RT} and E_g should be more sample dependent, since the concentration of the disorder should vary from sample to sample. But, in fact, these parameters are nearly independent of the sample. Contrary to one-dimensional organic conductors, the metallic state of the two-dimensional one is stable against the disorder in the anion layer. For example, such salts with orientational disorders, κ'-$Cu_2(CN)_3$[19] (CN disorder), β-I_2Br[38] (disorder of I_2Br), exhibit metallic transport properties.

The existence of a strong electron–electron correlation is suggested by the relatively large density of states obtained by the band calculation. This is also supported by the following three facts: i) The magnitude of χ_{spin} is about two-times larger than metallic BEDT–TTF salts. ii) The temperature dependence of χ_{spin} is represented by that of localized spins with an antiferromagnetic interaction. iii) The TEP along the stacking axis saturates towards 60 $\mu V K^{-1}$, which is the predicted value for a system with a 3/4-filled band and with large U and small V, compared to the band width. This prediction is also valid for a system with a 3/4-filled band and with both U and V being larger than the band width. The band structure calculated with the extended Hückel method cannot explain the semiconducting behavior of the title compound. This fact may also be due to the strong electron–electron correlation, which is not considered in the extended Hückel method.

This situation is just like the case of the Mott insulator, although the 3/4-filled band is not appropriate to this picture. To clarify the exact origin of the charge localization, a further investigation, for instance an optical measurement, is necessary.

In summary, the title compound is unique in the sense that this is the first magnetic insulator based on BEDT–$TTF^{+0.5}$ with uniform stacks in temperature regions a) and b), and undergoes strong dimerization and antiferromagnetic ordering in region c).

We acknowledge Dr. T. Mori for his advice concerning the band calculation and Professor N. Kojima for discussion about the magnetic properties. This work was supported by a Grant-in-Aid for Scientific Research from the Ministry of Education, Science and Culture and a Grant for the International Joint Research Project from the NEDO, Japan.

References

1) T. Ishiguro and K. Yamaji, "Organic Superconductors," Springer Verlag, Berlin (1990).

2) T. Sasaki, N. Toyota, M. Tokumoto, N. Kinoshita, and H. Anzai, *Solid State Commun.*, **75**, 93 (1990).

3) T. Sasaki, N. Toyota, M. Tokumoto, N. Kinoshita, and H. Anzai, *Solid State Commun.*, **75**, 97 (1990).

4) K. Oshima, T. Mori, H. Inokuchi, H. Urayama, H. Yamochi, and G. Saito, *Phys. Rev. B*, **38**, 938 (1988).

5) M. A. Beno, M. A. Firestone, P. C. W. Leung, L. M. Sowa, H. H. Wang, J. M. Williams, and M. -H. Whangbo, *Solid State Commun.*, **57**, 735 (1986).

6) S. D. Obertelli, R. H. Friend, D. R. Talham, M. Kurmoo, and P. Day, *J. Phys.: Condens. Matter*, **1**, 5671 (1989).

7) I. D. Parker, R. H. Friend, M. Kurmoo, and P. Day, *J. Phys.: Condens. Matter*, **1**, 5681 (1989).

8) M. Kurmoo, M. A. Green, P. Day, C. Bellitto, G. Staulo, F. L. Pratt, and W. Hayes, *Synth. Met.*, **55—57**, 2380 (1993).

9) T. K. Worthington, W. J. Gallagher, and T. R. Dinger, *Phys. Rev. Lett.*, **59**, 1160 (1987).

10) a) K. Oshima, H. Urayama, H. Yamochi, and G. Saito, *J. Phys. Soc. Jpn.*, **57**, 730 (1988); b) H. Ito, M. Watanabe, Y. Nogami, T. Ishiguro, T. Komatsu, G. Saito, and N. Hosoito, *J. Phys. Soc. Jpn.*, **60**, 3230 (1991).

11) T. Iwazumi, R. Yoshizaki, H. Sawada, H. Uwe, T. Sakudo, and E. Matuura, *Jpn. J. Appl. Phys.*, **26**, L383 (1987).

12) a) K. Holczer, D. Quinlivan, O. Klein, G. Grüner, and F. Wudl, *Solid State Commun.*, **76**, 499 (1990); b) K. Kanoda, K. Akiba, K. Suzuki, T. Takahashi, and G. Saito, *Phys. Rev. Lett.*, **65**, 1271 (1990).

13) Y. J. Uemura, L. P. Le, G. M. Luke, B. J. Sternlieb, W. D. Wu, J. H. Brewer, T. M. Riseman, C. L. Seaman, M. B. Maple, M. Ishikawa, D. G. Hinks, J. D. Jorgensen, G. Saito, and H. Yamochi, *Phys. Rev. Lett.*, **66**, 2665 (1991).

14) H. Yamochi, T. Komatsu, N. Matsukawa, G. Saito, T. Mori, M. Kusunoki, and K. Sakaguchi, *J. Am. Chem. Soc.*, **115**, 11319 (1993).

15) N. Kinoshita, M. Tokumoto, H. Anzai, and G. Saito, *Synth. Met.*, **19**, 203 (1987).

16) M. Tokumoto, H. Anzai, T. Ishiguro, G. Saito, H. Kobayashi, R. Kato, and A. Kobayashi, *Synth. Met.*, **19**, 215 (1987).

17) T. Mori and H. Inokuchi, *Solid State Commun.*, **59**, 355 (1986).

18) Y. Iwasa, K. Mizuhashi, T. Koda, Y. Tokura, and G. Saito, *Phys. Rev. B*, **49**, 3580 (1994).

19) T. Komatsu, T. Nakamura, N. Matsukawa, H. Yamochi, G. Saito, H. Ito, T. Ishiguro, M. Kusunoki, and K. Sakaguchi, *Solid State Commun.*, **80**, 843 (1991).

20) G. Sheldrick, "SHELX86 (1986) and SHELX76 (1976), Program for Crystal Structure Determibation," Univ. of Cambridge.

21) R. Comes, M. Lambert, and A. Guinier, *Acta Crystallogr., Sect. A*, **A26**, 244 (1970).

22) T. Mori, A. Kobayashi, Y. Sasaki, H. Kobayashi, G. Saito, and H. Inokuchi, *Bull. Chem. Soc. Jpn.*, **57**, 627 (1984).

23) R. B. Roberts, *Phil. Mag.*, **36**, 91 (1977).

24) "Chemistry Handbook," 3rd ed, ed by The Chemical Society of Japan, Maruzen, Tokyo (1984), pp. II-508 [in Japanese].

25) The equation used for the fitting procedure is

$$I=a_1(a_2-H)/[1+{a_3}^2(a_2-H)^2]^2 +a_4[1-{a_3}^2(a_2-H)^2]/[1+{a_3}^2(a_2-H)^2]^2 +a_5(a_2-H)+a_6,$$

where I is the first-derivative intensity and a_1—a_6 are the fitting parameters.

26) A. Weiss and H. Witte, "Magnetochemie," Verlag Chemie, Weinheim (1973).

27) H. Kobayashi, R. Kato, A. Kobayashi, Y. Nishio, K. Kajita, and W. Sasaki, *Chem. Lett.*, **1986**, 833.

28) K. Bender, I. Hennig, D. Schweitzer, K. Dietz, H. Endres, and H. J. Keller, *Mol. Cryst. Liq. Cryst.*, **108**, 359 (1984).

29) R. P. Shibaeva and R. M. Lobkovskaya, *Krystallografiya*, **33**, 408 (1988).

30) H. Mori, S. Tanaka, T. Mori, Y. Maruyama, H. Inokuchi, and G. Saito, *Solid State Commun.*, **78**, 49 (1991).

31) H. Mori, S. Tanaka, M. Oshima, G. Saito, T. Mori, Y. Maruyama, and H. Inokuchi, *Bull. Chem. Soc. Jpn.*, **63**, 2183 (1990).

32) P. M. Chaikin and G. Beni, *Phys. Rev. B*, **13**, 647 (1976).

33) T. Sugano, G. Saito, and M. Kinoshita, *Phys. Rev. B*, **34**, 117 (1986).

34) K. Nozawa, T. Sugano, H. Urayama, H. Yamochi, G. Saito, and M. Kinoshita, *Chem. Lett.*, **1988**, 617.

35) B. Rothaemel, L. Forró, J. R. Cooper, J. S. Schilling, M. Weger, P. Bele, H. Brunner, D. Schweitzer, and H. J. Keller, *Phys. Rev. B*, **34**, 704 (1986).

36) W. E. Hatfield, W. E. Estes, W. E. Marsh, M. W. Pickens, L. W. ter Haar, and R. R. Weller, "Extended Linear Chain Compounds," ed by J. S. Miller, Plenum Press, New York (1983), Vol. 3, Chap. 2, p. 45. The equation actually used is $\chi_{spin}(T)=(Ng^2{\mu_B}^2/k_BT)[(A+Bx+Cx^2)/(1+Dx+Ex^2+Fx^3)]$, where N is the number of spins per mol, μ_B the Bohr magneton, k_B the Boltzmann constant, $x=|J|/T$, and A—F are the constant parameters of $A=0.25$, $B=0.14995$, $C=0.30094$, $D=1.9862$, $E=0.68854$, and $F=6.0626$. T and J are in units of K and χ_{spin} in units of emu mol^{-1}.

37) G. S. Rushbrooke and P. J. Wood, *Mol. Phys.*, **1**, 257 (1958).

38) E. L. Venturini, J. E. Schirber, H. H. Wang, and J. M. Williams, *Synth. Met.*, **27**, A243 (1988).